International Journal of Mechanical and Electrical Engineering
ISSN: 3005-9615 (Print), ISSN: 3005-7132 (Online) | Volume 8, Number 3, Year 2026
DOI: https://doi.org/10.62051/ijmee.v8n3.07
Journal homepage: https://wepub.org/index.php/IJMEE/index

Design and Analysis of Impeller for Ducted Axial-flow Turbine in Natural Gas Power Generation Systems

Dongming Gao, Ran Zhang *, Lide Wu, Hua Fan

College of Mechanical Engineering, Xihua University, Chengdu, Sichuan, China
* Corresponding Author: Ran Zhang

ABSTRACT

Natural gas pressure difference power generation is an innovative low-carbon energy technology that integrates energy efficiency, environmental protection, and economic benefits. This paper proposes a ducted natural gas pressure energy power generation device using an axial-flow turbine. The geometric parameters of the rotor and stator blades of the axial-flow turbine are derived through a one-dimensional design method. Additionally, the flow characteristics and blade load distribution of this blade profile are analyzed, and directions for further optimizing the turbine to enhance its output power are put forward.

KEYWORDS

Pressure Energy Power Generation; Axial-flow Turbine; Numerical Simulation.

1. INTRODUCTION

Natural gas, as a clean energy source, is being increasingly widely used in the energy sector [1].Its share in fossil fuels is growing increasingly larger [2].To ensure the safe supply and use of natural gas, pressure reducing valves are required to reduce the pressure of high-pressure natural gas to a specified level, which results in the waste of pressure energy [3]. Relevant studies have shown that when 1 m^3 of natural gas is depressurized from 10 MPa to 0.8 MPa, the maximum recoverable pressure energy is 359.12 kJ [4]. Taking a gate station with a daily processing capacity of 500,000 m^3 as an example, when the pressure drops from 4.0 MPa to 0.4 MPa, the pressure energy loss is approximately 101.7 MJ/h, resulting in an annual direct economic loss of 26.52 million RMB [5]. This indicates that the pressure energy in natural gas pipeline networks has enormous utilization potential [6].However, external expansion machines require a large amount of space, and due to the presence of a coupling, the risk factor increases[7].This paper proposes a ducted natural gas pressure energy generation device using an axial-flow turbine.

2. DUCTED AXIAL-FLOW TURBINE DESIGN

The selection for the turbine blade median diameter is 100mm, the number of stator blades is 19, and the number of rotor blades is 24. The selected rated rotational speed of the turbine is 38,000 r/min. The inlet mass flow rate m=7kg/s, inlet total pressure P=1.7Mpa, and inlet total temperature T_0=300K.

Through geometric parameter calculation, the velocity triangle at the mid - diameter of the turbine blade is obtained as shown in Fig. 1.

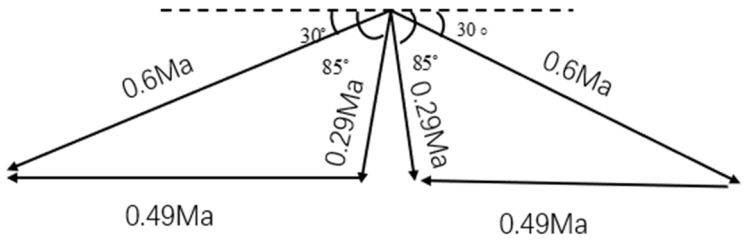

Fig 1. Velocity Triangle at The Mid-diameter of The Blade Shape

The inlet and outlet geometric angles of the stator and rotor blades are derived from the inlet and outlet flow angles in the reference velocity triangle. The one-dimensional design results of the blade geometric parameters are shown in Table 1.

Table 1. Blade Profile Geometric Parameters

Geometric parameters	Stator	Rotor
Outer diameter/mm	120	120
Inner diameter/mm	80	79
Chord length/mm	20.63	16.25
Axial chord length/mm	14.27	14.63
Inlet geometry Angle/°	90	85
Exit geometric Angle/°	30	30
Flow channel form	Equal outer diameter	

Common parametric blade modeling methods include the mid-curve plus thickness distribution method [8] and the method of determining the suction surface and pressure surface profiles separately [9,10]. This paper uses the mid-curve plus thickness distribution method for blade modeling. The mid-curve of the blade is constructed by a quadratic Bezier curve based on the actual chord length (1). The thickness distribution of the blade follows the symmetrical distribution pattern of the CFtubo AT-P series.

$$B(t) = (1-t^2)\mathrm{P}_0 + 2t(1-t)\mathrm{P}_1 + t^2\mathrm{P}_2, t \in [0,1] \tag{1}$$

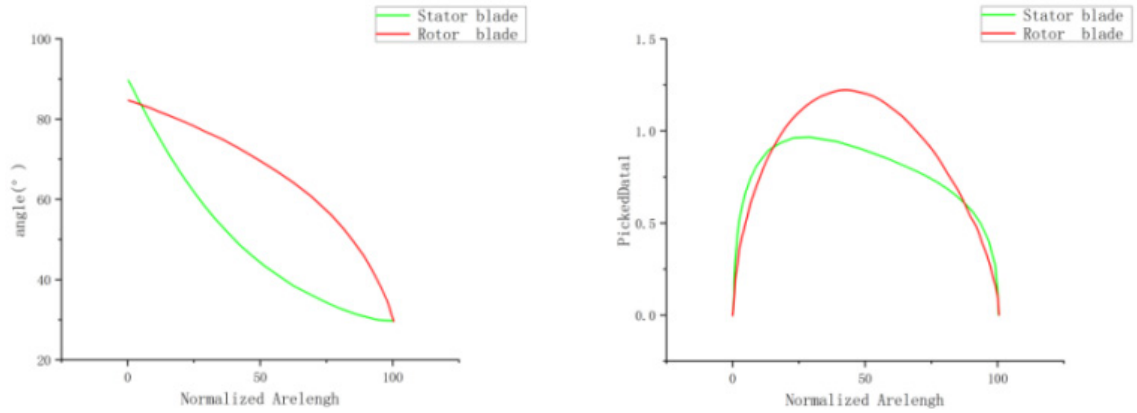

(a) Angular Distribution Pattern (b) Thickness Distribution Pattern

Fig 2. Angular Distribution Schematic of Mean Camber Line at Mid-diameter Along The Blade

Among them, P_0 and P_2 are determined by the chord length and the axial chord length, and the control point P_1 is determined by the inlet and outlet geometric angles. Fig. 2 shows the schematic diagram of the camber line and thickness distribution at the mid - diameter of the turbine stator and rotor blades.

3. ANALYSIS OF DUCTED AXIAL-FLOW TURBINE

Computational Fluid Dynamics (CFD), as a more advanced method, has gradually become a means of analyzing gas dynamics [11].In this paper, the mesh generation is carried out using TurboGrid, the mesh partitioning software integrated within ANSYS. As shown in Fig. 3, The domain was divided into rotating, stationary regions, and interfaces. The rotational speed was set to 38,000 rpm.The inlet boundary condition for the import is selected as a pressure inlet. The inlet air temperature is set at 300K and the inlet pressure at 1.7 MPa. The air flow direction is axial. The outlet mass flow rate is set to 7 kg/s for the entire flow channel.Taking the default mesh count of 40,000 in TURBOGRID as the initial value, with an incremental step size of 10,000, the variation in calculation results began to decrease sharply once the mesh count reached 100,000. The change in the calculated turbine output power was within 0.8%; therefore, a mesh count of 100,000 was adopted as the benchmark for mesh division density.

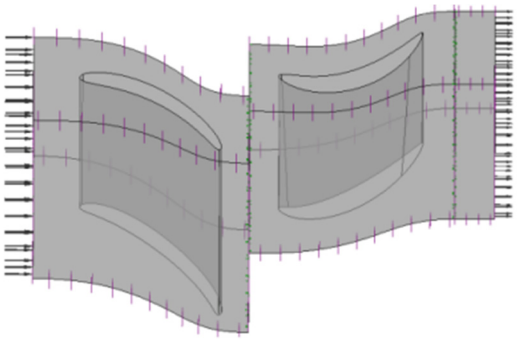

Fig 3. Computational Domain Division in CFX-Pre

3.1. Blade Profile Flow Analysis

(a)At 10% Blade Height (b)At 50% Blade Height (c)At 90% Blade Height

Fig 4. Mach Number Distribution Nephogram

Fig. 4 presents Mach number distribution nephograms at different blade heights of the blade profile. As shown in Fig. 4(b), the velocity distribution at the mid-diameter of the blade profile is in good agreement with the results of the calculated velocity triangle. The velocity distribution in the flow channel at this blade height is relatively uniform, indicating good overall fluid flow.As can be seen from Fig. 4(a) and 4(c), the blade profile exhibits a higher degree of expansion at the root of the stator blade. However, overall, the fluid is far from reaching a critical state in the blade profile, and the degree of fluid expansion is not significant. The maximum Mach number at the outlet of the stator blade is only 0.6725. If the flow channel area is further reduced to increase the degree of expansion, the fluid can obtain more kinetic energy, thereby increasing the overall power output of the turbine.

At 90% blade height, partial low-velocity regions appear on the pressure surface of the rotor blade leading edge.

Fig. 5 shows the fluid trace diagrams near the rotor blades at different blade heights. As can be seen from Fig. 5(b), the inlet direction of the airflow at 50% blade height is close to the calculated value. Therefore, the geometric angle at the inlet of the rotor blade at 50% blade height is reasonable, and the airflow does not separate on the pressure and suction surfaces of the impeller, resulting in small flow losses of the gas.As shown in Fig. 5(a) and 5(c), at 10% blade height, the airflow has a large positive incidence angle at the leading edge of the rotor blade, causing the airflow to separate prematurely near the trailing edge of the suction surface. This will generate additional flow losses. At the blade tip, the airflow has a large negative incidence angle, which makes the rotor blade bear greater loads at the leading edge and causes a large-area separation region of the airflow at the leading edge of the pressure surface of the rotor. This leads to significant flow losses and leading-edge losses near the blade tip of the rotor blade.This is due to the mismatch between the geometric angles at the stator outlet and rotor inlet at the blade tip and root. A two-section blade twist can be implemented to individually adjust the inlet and outlet geometric angles at the tip and root.Further improve the conversion efficiency of pressure energy [12].

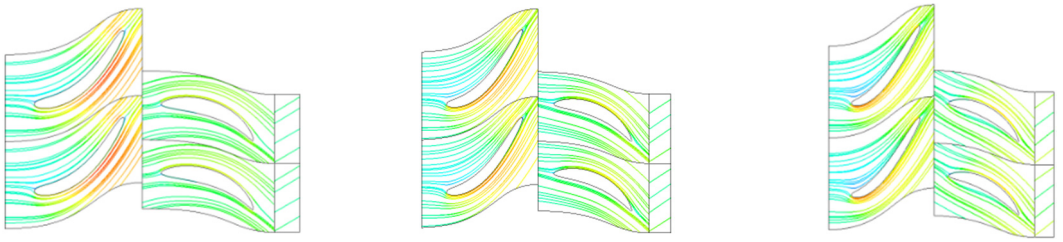

(a)At 10% Blade Height (b)At 50% Blade Height (c)At 90% Blade Height

Fig 5. Fluid Trace Diagram

3.2. Blade Surface Load Distribution

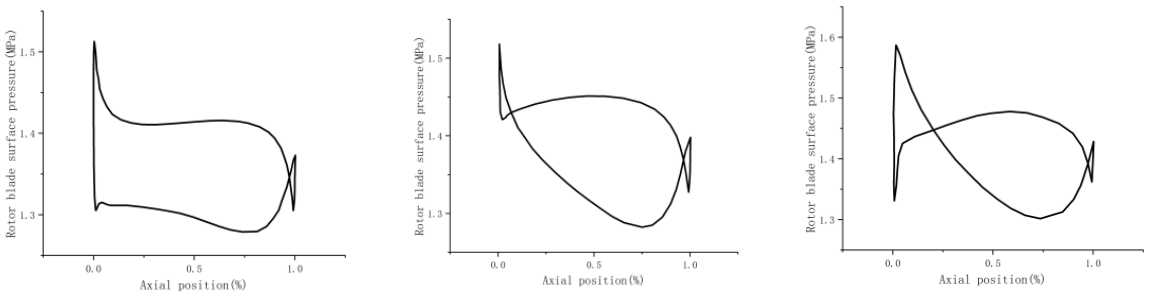

(a)At 10% Blade Height (b)At 50% Blade Height (c)At 90% Blade Height

Fig 6. Pressure Distribution Law on Blade Surface at Different Blade Heights

Fig. 6 shows the pressure distribution on the blade surface at different blade heights of the blade profile. It can be seen from the figure that the pressure load on the surface of the rotor blade exhibits fluctuations near the inlet and outlet, and the fluctuations in the pressure distribution at the rotor inlet increase significantly with the increase in blade height.

This is because the circumferential velocity of the turbine blade gradually increases along the blade height, and the inlet angle of the airflow into the rotor blade also changes along the blade height. However, the blade profile is designed only according to the velocity triangle at the mean diameter and adopts a straight blade form. Therefore, when the airflow at each blade height enters the rotor

blade, it will produce impact phenomena of different degrees. In the lower part of the blade, the airflow generally impacts the pressure surface, while in the upper part of the blade, it impacts the suction surface [13].

To further illustrate this phenomenon, Fig. 7 presents the pressure distribution nephogram at the leading edge of the rotor blade. As shown in the figure, influenced by the airflow impact at the leading edge of the rotor blade, a high-pressure region appears on the suction surface of the leading edge in the blade tip to mid-diameter area. As the blade height decreases, the high-pressure region gradually diminishes. Similarly, partial high-pressure regions also exist on the pressure surface of the leading edge in the blade root to mid-diameter area.

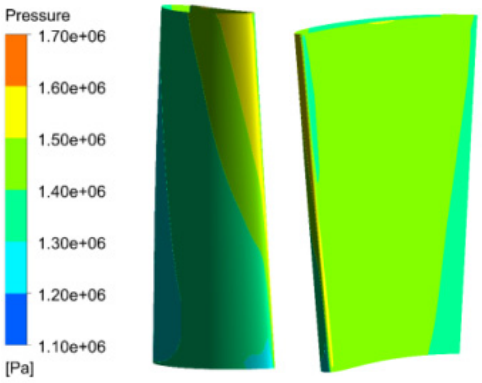

Fig 7. Pressure Distribution Nephogram on The Leading Edge Surface of Rotor Blade

4. SUMMARY

The one-dimensional design method determined that the axial-flow turbine has an outer diameter of 120 mm for both the rotor and stator blades, with the rotor inner diameter being 79 mm and the stator inner diameter 80 mm. The rotor inlet geometric angle is 85°, the stator inlet geometric angle is 90°, and the outlet geometric angles of both the rotor and stator are 30°. Additionally, the rotor chord length is 16.25 mm, while the stator chord length is 20.63 mm.

The analysis of the blade profile's flow characteristics shows that the flow performance at the mid-diameter is close to the computational results. The stator blade root exhibits a higher degree of expansion, and the airflow at the leading edge of the rotor blade root has a larger positive incidence angle. In contrast, the airflow at the rotor blade tip has a larger negative incidence angle, and partial low-velocity regions appear on the pressure surface of the leading edge. The analysis of the blade surface load distribution reveals that the pressure load on the rotor blade surface fluctuates near the inlet and outlet. Moreover, as the blade height increases, the fluctuation of the pressure distribution at the rotor inlet significantly intensifies.

The optimization directions for the device are proposed. Specifically, the inlet and outlet geometric angles at the blade tip and root can be adjusted individually to induce blade twist, thereby reducing energy losses and enhancing power output.

REFERENCES

[1] Yu, Y., et al., Operational Energy Efficiency Analysis and Optimization of Natural Gas Pressure Difference Power Generation, Chemical Engineering of Oil & Gas, 53(2024), 5, pp. 129-137.

[2] Cetiner, I., et al., Cost Based Optimization of Industrial Bulk Compresed Natural Gas Filling Facility Operations, Thermal Science, 25(2021), 6, pp. 4721-4735.

[3] Xu, X., et al., Potential Analysis of Pressure Energy Recovery and Utilization in Chuanqi East Transmission Substations, Natural Gas Technology and Economy, 7(2013), 2, pp. 48-51+79.

[4] Wang, Y., et al., Application of Natural Gas Pressure Difference Power Generation Technology in Pressure Regulation Gate Stations, Energy Conservation in Petroleum & Petrochemical Industry, 8(2018), 5, pp. 9-11+18.

[5] Wang, Z P., et al., Study on Pressure Energy Recovery and Utilization in Natural Gas Pipeline Networks, Gas & Heat, 40(2020), 1, pp. 14-16+44-45.

[6] Zhang, R., et al., Research on The Process Flow of Natural Gas Differential Pressure Power Generation System, Thermal Science, 29(2025), 2, pp. 1115-1121.

[7] Zhang, R., et al., Optimization Research on Plant Key Parameters of The Impeller of The Ducted Natural Gas Pressure Power, Thermal Science, 29 (2025), 2, pp. 1101-1106.

[8] Koini, G. N., A Software Tool for Parametric Design of Turbomachinery Blades, Advances in engineering software, 40(2019), 1, pp. 41-51.

[9] Li, J. B., et al., Turbine Blade Aerodynamic Design Software, Gas Turbine Test and Research, 24(2011), 3, pp. 11-15.

[10] Pritchard, L. J., An Eleven Parameter Axial Turbine Airfoil Geometry Model, American Society of Mechanical Engineers, 1(1985), March, pp. 12-13.

[11] Vilotijevic, V., et al., Aerodynamic Analysis of Field Wind Turbine: A Comparative Study of Computational Methods with Experimental Validation, Thermal Science, 29 (2025), 2, pp. 1607-1618.

[12] Li, Y B., et al., Correction Strategy for Blade Installation Angle of Nuclear Main Pump Considering Pre-Swirl Characteristics, Journal of Xihua University (Natural Science Edition), 44(2025), 2, pp. 1-10+135.

[13] Shen, S Y., et al., Principles of Steam Turbines, China Electric Power Press, Beijing, 1992.